Acta Astronautica 87 (2013) 40–47

Contents lists available at SciVerse ScienceDirect

Acta Astronautica

journal homepage: www.elsevier.com/locate/actaastro

A graph-theory approach to designing deployable mechanism of reflector antenna

C.M. Feng, T.S. Liu *

Department of Mechanical Engineering, National Chiao Tung University, Hsinchu 30010, Taiwan

ARTICLE INFO

Article history:
Received 8 September 2012
Received in revised form
22 January 2013
Accepted 27 January 2013
Available online 8 February 2013

Keywords:
Reflector antenna
Deployable antenna design
Graph theory
Flow value method
Kinematic chain
Deployable mechanism

ABSTRACT

The objective of this paper is to present an exhaustive search method for designing new deployable mechanisms of reflector antennas. The procedure is based on the graph theory and a flow value method. The mechanism is composed of links and joints. Connections between links are represented by using the graph theory. Rules representing design criteria and the flow value method based on load flow are taken into account to evaluate and select mechanisms among those that are enumerated in the database. Finally, this study presents a deployable mechanism that transmits load the most efficiently.

1. Introduction

Many deployable mechanisms, such as folding chairs, umbrella, or deployable reflector antenna for telecommunications, are useful to human life. All of these deployment mechanisms share the same characteristics; that is, the packaged configuration should be as small as possible. Deployable mechanisms are widely used in space technologies. Construction in a low-gravity or no-gravity environment is quite difficult. Hence, some space structures, such as a shelter, is designed as deployable assemblies [1]. Solar panels, antennas, radars, and masts of the satellites are generally deployable to keep the device compact during launch. Similarly, various types of appendages are desired to be deployable for the same reason [2]. For space applications, a deployable antenna is seriously limited by many constraints, such as the mass, stowed size, and the size after deployed. Most of deployable antennas can be roughly divided into two types: solid surface antennas [3–5] and membrane surface antennas [6–8]. An umbrella-type concept may be the most popular one among membrane antennas and is the first to exceed the barrier of a solid reflector [8]. Many deployable antennas in orbit use this kind of structure [9–11]. Some studies on the umbrella-type antenna have been developed, such as radiation characteristics [12], packaging models [13], and designing composite ribs [14]. However, to the authors' knowledge, there has been no systematic procedure proposed to designing mechanisms of deployable antennas. Liu and Chou [15] used the graph theory and a flow value method to carry out creative design of vehicle suspension. This study aims to develop an exhaustive search procedure, which belongs to a creative design method, for designing deployable antennas. A deployable mechanism of antennas is composed of links. The graph theory [16] is used to graphically represent connections among links and the flow value method is used to evaluate and select mechanisms among those that are enumerated in the database. The advantages of this method include not only exhaustive search for alternative designs, but also acquiring representative design

* Corresponding author. Tel.: +886 3 5712121x55123; fax: +886 3 5720634.
E-mail address: tsliu@mail.nctu.edu.tw (T.S. Liu).

0094-5765/$ - see front matter © 2013 IAA. Published by Elsevier Ltd. All rights reserved.
http://dx.doi.org/10.1016/j.actaastro.2013.01.019

that possesses good capability for load transmission. Finally, the resultant mechanism possesses attributes of load transmission efficiency, small area of storage, large area after deployment, and amenable to actuation.

2. Deployable reflector antenna

In ring-like arrangement as shown in Fig. 1, the mechanism of deployable reflector antennas consists of many identical linkages of one degree-of-freedom. Since the linkages are in cyclic arrangement, the reflector antenna will produce a hole in the center. The hole is filled with a rigid reflector which does not have any changeable profile in the deployment process. Each linkage includes a parabolic rib that is used in conjunction with other linkages to form parabolic surface of reflection electromagnetic wave. Every parabolic rib is treated as an output member and is driven by a spring sleeve. Fig. 2 illustrates a deployment process of the antenna. Every rib has to move a large angle during deployment. If this linkage comprises four links, the spring sleeve requires a long stroke that would extend the sleeve length and hence increase the linkage size. Accordingly, in this study every linkage is synthesized by using six links rather than four links.

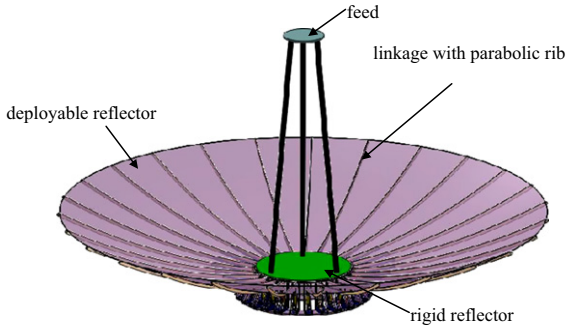

Fig. 1. Deployable reflector antenna composed of 27 identical linkages.

3. Design criteria

This section presents design criteria for kinematic linkages in developing deployable mechanisms of a reflector antenna. In order to calculate the number of degrees of freedom of one linkage that can be regarded as planar motion, Suh and Radcliffe [17] proposed a mobility criterion formula known as

$$f = 3(L-1)-2J_1-J_2 \tag{1}$$

where

f=total degrees of freedom in the linkage.
L=number of links.
J_1=number of lower pairs, which represents kinematic pairs with one degree of freedom [17].
J_2=number of higher pairs, which represents kinematic pairs with two degree of freedom [17].

In the current study, the six-link mechanism contains no higher pair. Hence, substituting $f=1$, $L=6$, and $J_2=0$ into Eq. (1) leads to

$$1 = 3(6-1)-2J_1-0$$

Therefore, $J_1=7$. Based on this result, the linkage contains seven lower pairs. Denote the numbers of binary links, ternary links, and quaternary links of each six-link linkage as B, T, and Q, respectively. Fig. 3 illustrates the types of theses links [18].

The total number of links in this linkage has to satisfy

$$B+T+Q = L = 6 \tag{2}$$

Since one joint is composed of two link nodes, and [18]

$$\text{nodes} = \textit{order of link} \times \textit{No. of links of that order} \tag{3}$$

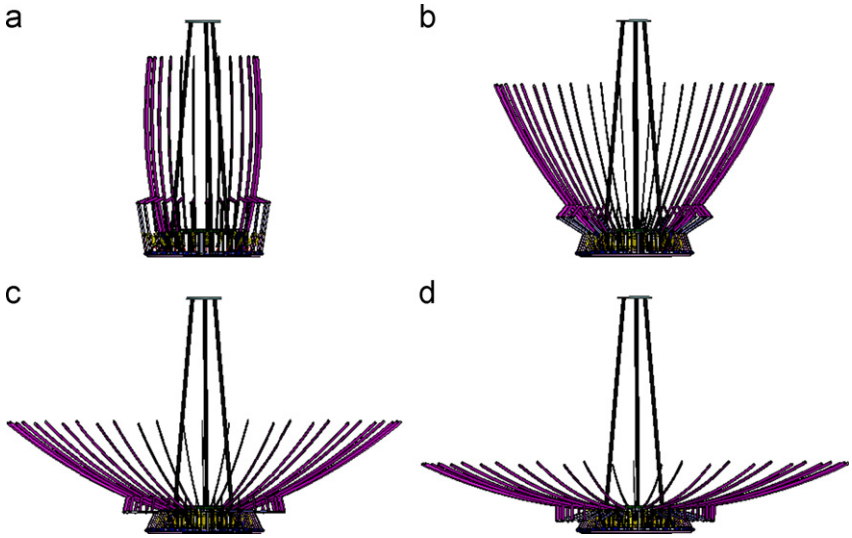

Fig. 2. Deployment process of the deployable reflector antenna with 27 ribs in purple color: (a) folded state, (b) and (c) deployed process, (d) fully deployed state. (For interpretation of the references to color in this figure legend, the reader is referred to the web version of this article.)

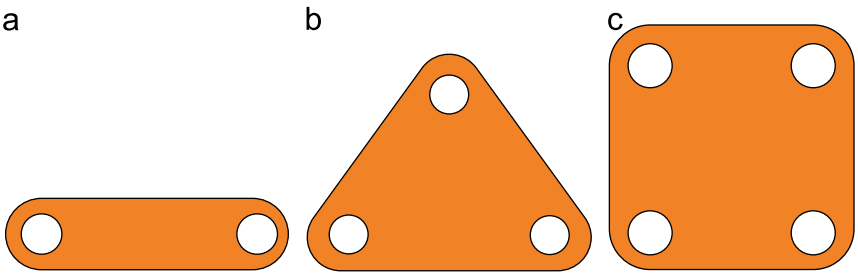

Fig. 3. Three types of different links: (a) binary link, (b) ternary link, and (c) quaternary link.

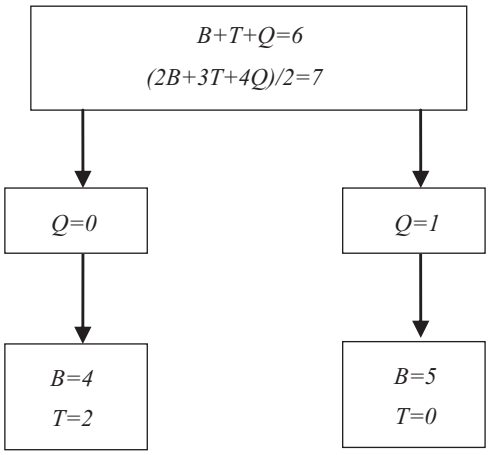

Fig. 4. Two kinematic conditions: $Q=0$, $B=4$, $T=2$ and $Q=1$, $B=5$, $T=0$ obtained from solving Eqs. (2) and (4). The first condition leads to a six-link linkage with four binary links and two ternary links; while the other condition yields another six-link linkage with one quaternary link and five binary links.

where *order of link* means that the number of nodes in this link, one has

$$\frac{(2B+3T+4Q)}{2} = J_1 = 7 \tag{4}$$

Calculated results are shown in Fig. 4, in which only two kinematic conditions satisfy both Eqs. (2) and (4). Accordingly, the first condition $Q=0$, $B=4$, and $T=2$ represents a six-link linkage consisting of four binary links and two ternary links; the other condition $Q=1$, $B=5$, and $T=0$ represents the other six-link linkage comprising one quaternary link and five binary links.

According to Fig. 4, enumeration generates eight types of kinematic chains as shown in Fig. 5. Fig. 5(e)–(h) are regarded as four links kinematic chains since each of them includes a subchain formed by three links that altogether behave as a rigid body. Therefore, these four types are not suitable for use. The other four types of feasible six links kinematic chains are illustrated in Fig. 4(a)–(d). Dealing with the four feasible types, the following design criteria are prescribed:

(1) The spring sleeve cannot become the ground link, denoted as G. Otherwise, designing the mechanism may become difficult.
(2) The ground link has to be a ternary link to reduce the number of the floating links in the mechanism.
(3) In order to avoid the profile of the rigid reflector region during deployment to produce changes, the parabolic rib, denoted as r, must be adjacent to the ground link.
(4) One of the two spring sleeve links has to be hinged to the ground links. Otherwise, this design could increase the complexity.
(5) The spring sleeve consists of a piston, denoted as p and a cylinder, denoted as c. The joint connecting these two links is treated as a translational joint.
(6) The translational joint cannot be a multiple joint. Otherwise, the spring sleeve is easy to cause wear.
(7) In order to avoid producing redundant links, the ground, the rib, and the spring sleeve cannot become a four-link loop.

After eight mechanisms in Fig. 5 are screened, only three remain as depicted in Fig. 6. Fig. 5(d) is ruled out since it does not pass criteria (2). In addition, Fig. 5(e)–(h) are ruled out since each of them contains a three-link subchain that behaves like a rigid body.

4. Graph representation

Graph representation is used in this study to describe the topological structure of mechanisms, and the topological structure will be used to construct a flow path graph in Section 5. The topological structure of a mechanism is characterized by types, numbers of mechanical members, joints, and connection or not between members. Hence, based on the graph theory, the mechanisms in Fig. 6 can be represented by graphs illustrated in Fig. 7 respectively.

In Fig. 7, vertices denote links in mechanisms, while edges represent joints in mechanisms. Link numbers from one to six are prescribed arbitrarily. The topological structure of each mechanism in Fig. 6 is represented by a graph in Fig. 7 and the graph is expressed as a matrix. The matrix of a linkage with n links is a $n \times n$ matrix, in which diagonal elements m_{ii} symbolize the type of linkage member i. Being a symmetric matrix

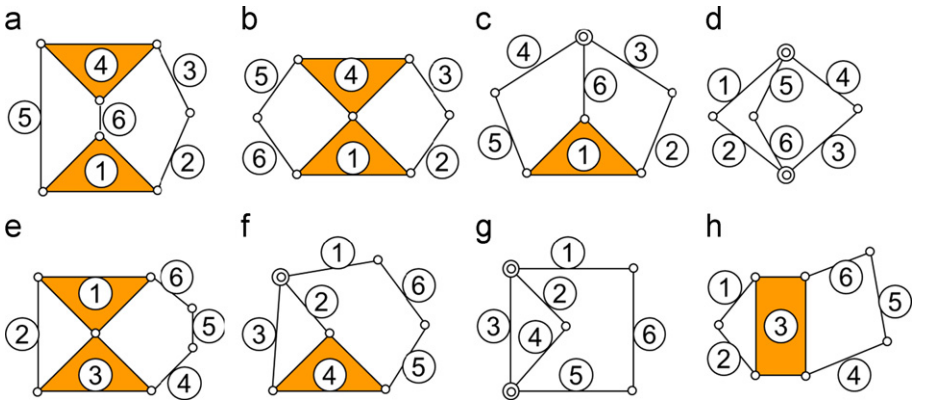

Fig. 5. (a), (b), and (e) six-link linkage with two ternary links, (c) six-link linkage with one ternary link, (d) and (g) six-link linkage with two multiple joints, (f) six-link linkage with one ternary link and one multiple joint, (h) six-link linkage with one quaternary link.

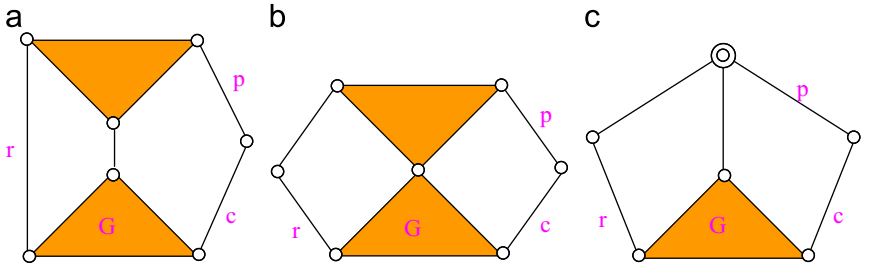

Fig. 6. Three mechanisms (a)–(c) obtained from screening eight mechanisms in Fig. 5. (d) is ruled out since it does not pass criteria (2). In addition, Fig. 5(e)–(h) are ruled out since each of them contains a three-link subchain that behaves like a rigid body.

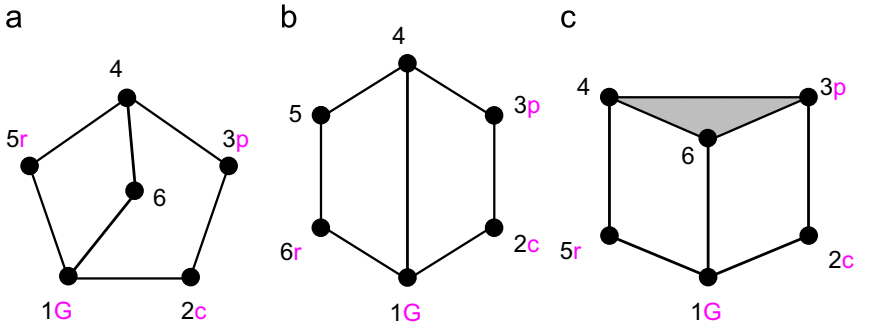

Fig. 7. Graph representations corresponding to three mechanisms in Fig. 6 respectively. The shade in (c) represents a link with three joints at 3, 4, and 6, unlike the other links that have two joints.

with $m_{ij}=m_{ji}$, an upper right non-diagonal element m_{ij} and a lower left non-diagonal element m_{ji} denote joints where the member i connects member j. If members i and j do not connect, $m_{ij}=m_{ji}=0$. As depicted in Fig. 7(a), the mechanism has six links and seven joints. G as link 1 denotes the ground link, c as link 2 denotes the cylinder, p as link 3 denotes the piston, L_4 as link 4 denotes the connecting link, r as link 5 denotes parabolic rib, and L_6 as link 6 denotes the connecting link. The topological matrix $M_T^{(a)}$of the mechanism shown in Fig. 6(a) can be written as

$$M_T^{(a)}=\begin{bmatrix} G & R & 0 & 0 & R & R \\ R & c & T & 0 & 0 & 0 \\ 0 & T & p & R & 0 & 0 \\ 0 & 0 & R & L_4 & R & R \\ R & 0 & 0 & R & r & 0 \\ R & 0 & 0 & R & 0 & L_6 \end{bmatrix} \tag{5}$$

Consider another mechanism configuration, Fig. 6(b). The topological matrix $M_T^{(b)}$ of the mechanism is expressed as

$$M_T^{(b)} = \begin{bmatrix} G & R & 0 & R & 0 & R \\ R & c & T & 0 & 0 & 0 \\ 0 & T & p & R & 0 & 0 \\ R & 0 & R & L_4 & R & 0 \\ 0 & 0 & 0 & R & L_5 & R \\ R & 0 & 0 & 0 & R & r \end{bmatrix} \tag{6}$$

In a similar manner, the topological matrix of Fig. 6(c) can be written as

$$M_T^{(c)} = \begin{bmatrix} G & R & 0 & 0 & R & R \\ R & c & T & 0 & 0 & 0 \\ 0 & T & p & R & 0 & R \\ 0 & 0 & R & L_4 & R & R \\ R & 0 & 0 & R & r & 0 \\ R & 0 & R & R & 0 & L_6 \end{bmatrix} \tag{7}$$

where R represents a revolute joint and T translational joint. These topological matrices represent connection properties among links.

5. Flow value method

Any of the three mechanisms depicted in Fig. 6 can be used as a deployable mechanism of the reflector antenna. Selecting the most suitable one is the major step in the creation of a new deployable antenna. In order to select the best design form the three candidate mechanisms, a flow value method [15] is used. The flow value method is a method based on load flow. In Fig. 7, the vertices and edges of a graph are analogous to tanks and pipelines, respectively. Load transmission from an input link to an output link can be treated as a liquid flow through pipelines. In this tank and pipeline system, the liquid flows through pipes. The shorter the pipes are, the less friction energy loss pipes cause. In a similar manner, the load loss occurs in links of kinematic linkages. When load transmits through two adjacent links, transmitting load decreases, which is arisen from link flexibility, backlash, and friction. If the loss at a joint is expressed as e, the load transmitted to next link is written as $1-e$. Assuming the loss is small and there are n

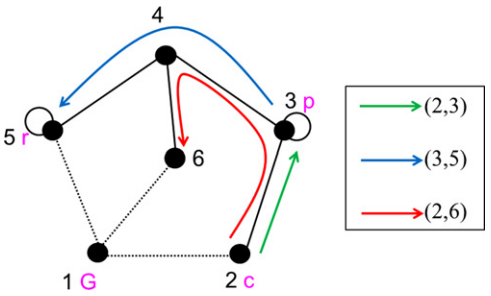

Fig. 10. Graph of the shortest flow paths corresponding to elements (2,3), (3,5), and (2,6) in Eq. (9).

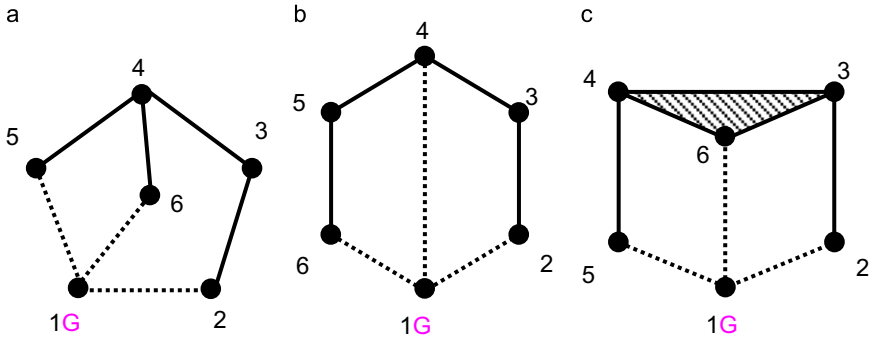

Fig. 8. Graphs (a)–(c) obtained from Fig. 7. The ground link G has no motion flow through the joints of ground link, i.e., paths leading to the ground link are removed. Dotted lines in (a)–(c) thus represent cutoff paths.

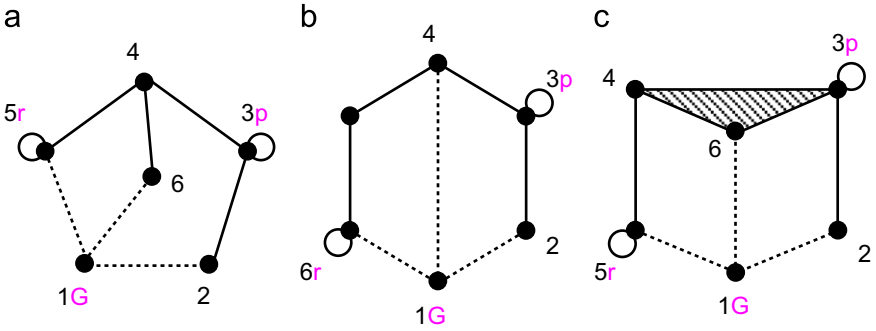

Fig. 9. Flow path graphs of deployable mechanism with input link p and output link r denoted as self-loop paths. The number of the paths is increased by one whenever the flow crosses a self-loop path.

distances in series at one path, the load transmitted will be

$$(1-e)^n \approx (1-ne) \tag{8}$$

where ne is the total loss.

In the flow value calculation, the ground link is treated as a fixed link which has no motion flow through the joints of this link. Since no motion flow at the joints of the ground link, all neighboring edges of the ground link in the graph can be deleted. In Fig. 7(a), link 1 is a ground link, i.e., paths between links 1–2, 1–5, and 1–6 are cutoff. This can be reflected in the graph by deleting the edges between the vertices 1–2, 1–5, and 1–6, while leaving the vertex 1 isolated, as shown in Fig. 8(a). Similarly, the adjacent edges of the ground link will be removed from the graphs in Fig. 7(b) and (c). The results are shown in Fig. 8(b) and (c).

In this study, the input link is defined as a link producing its own motion, and the output link transmits motion to itself. This in a graph can be represented by a self-loop at the vertices corresponding to the input link and output link [19]. In this study, the loads are generated by the spring sleeve, and finally transmitted to the rib. Thus, one of two links for the spring sleeve will be regarded as the input link, and the rib can be treated as the output link. Fig. 9 depicts three flow path graphs with the ground link G, input link p, and output link r.

The flow path in mechanism can be expressed by a matrix. Every element in the flow matrix is represented as a distance between two vertices in the graph. The distance is defined as the least number of edges to be crossed from one vertex to another. As shown in Fig. 9(a), since link 1 is a ground link, there is no load flow through link 1. The edges adjacent to link 1 are deleted, i.e., the edges that connect to link 1 cannot be the paths in counting the distance. Links 3 and 5 are input and output links, a self-loop is given for each of the input and output links in the flow path. In determining the elements of the flow matrix, the flow value is increased by one whenever the flow crosses a self-loop. According to the Fig. 9(a), the flow matrix $M_f^{(a)}$ can be written as

$$M_f^{(a)} = \begin{bmatrix} 0 & 0 & 0 & 0 & 0 & 0 \\ 0 & 0 & 1 & 3 & 4 & 4 \\ 0 & 1 & 1 & 1 & 2 & 2 \\ 0 & 3 & 1 & 0 & 1 & 1 \\ 0 & 4 & 2 & 1 & 1 & 2 \\ 0 & 4 & 2 & 1 & 2 & 0 \\ 0 & 12 & 7 & 6 & 10 & 9 \end{bmatrix} \boxed{44} \tag{9}$$

It follows from Eq. (8) that shortest paths provide the most efficient load transmission, which is desired in mechanism design. In the flow matrix, each element represents the number of edges along the shortest path. For example, Fig. 10 depicts the shortest paths of elements (2,3), (3,5), and (2,6) in Eq. (9). Thus, three matrix elements are $M_f^{(a)}(2,3)=1$, $M_f^{(a)}(3,5)=2$, and $M_f^{(a)}(2,6)=3+1=4$.

The sum of all the elements in the matrix give the flow value of this mechanism $0+12+7+6+10+9=44$.

Consider another mechanism configuration, Fig. 9(b). Link 1 is the ground link, link 3 is the input link, and link 6 is the output link. The flow matrix is expressed as

$$\begin{bmatrix} 0 & 0 & 0 & 0 & 0 & 0 \\ 0 & 0 & 1 & 3 & 4 & 5 \\ 0 & 1 & 1 & 1 & 2 & 3 \\ 0 & 3 & 1 & 0 & 1 & 2 \\ 0 & 4 & 2 & 1 & 0 & 1 \\ 0 & 5 & 3 & 2 & 1 & 1 \\ 0 & 13 & 8 & 7 & 8 & 12 \end{bmatrix} \boxed{48} \tag{10}$$

and the sum of all the elements give the flow value of this mechanism as 48, in a manner similar to Eq. (9).

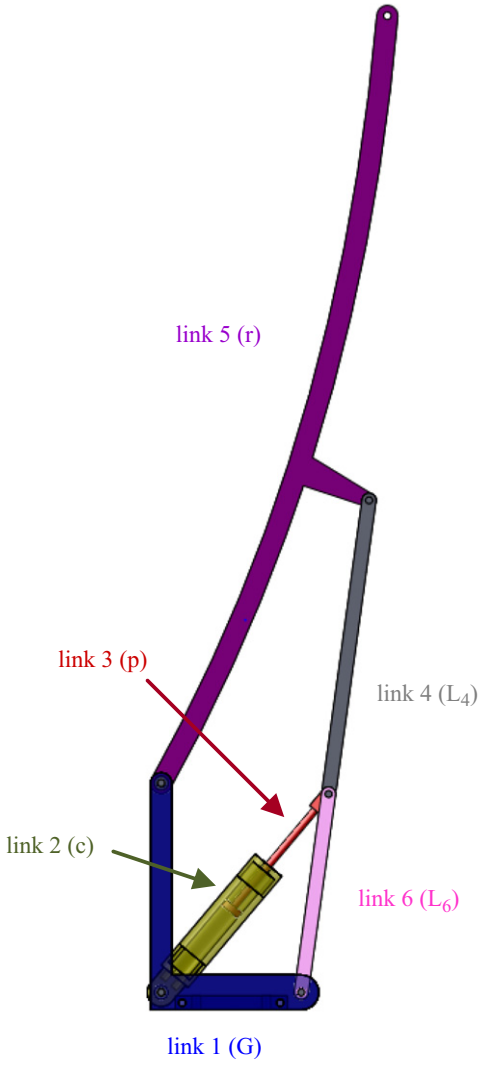

Fig. 11. Linkage corresponding to mechanism in Fig. 6(c). The symbols G, c, p, L_4, r, and L_6 represent the diagonal elements in Eq. (7). The diagonal elements mean the type of linkage member.

In a similar manner, the flow matrix of Fig. 9(c) can be written as

$$\begin{bmatrix} 0 & 0 & 0 & 0 & 0 & 0 \\ 0 & 0 & 1 & 3 & 4 & 3 \\ 0 & 1 & 1 & 1 & 2 & 1 \\ 0 & 3 & 1 & 0 & 1 & 1 \\ 0 & 4 & 2 & 1 & 1 & 2 \\ 0 & 3 & 1 & 1 & 2 & 0 \end{bmatrix} \quad (11)$$

$$\begin{matrix} 0 & 11 & 6 & 6 & 10 & 7 & \boxed{40} \end{matrix}$$

and the sum 40 of all the elements is calculated as the flow value of this mechanism, in a manner similar to ;Eq. (9).

The definition of flow values aims to provide criteria for evaluating performance of enumerated mechanisms at a conceptual design stage. The three mechanisms in Fig. 6, the flow values are 44, 48, and 40, respectively. The mechanism in Fig. 6(c) has a shorter flow distance than the other two. Therefore, this mechanism transmits load the most efficiently.

6. Conclusion

The mechanism in Fig. 6(c) has been determined by the present method to be one linkage in the deployable

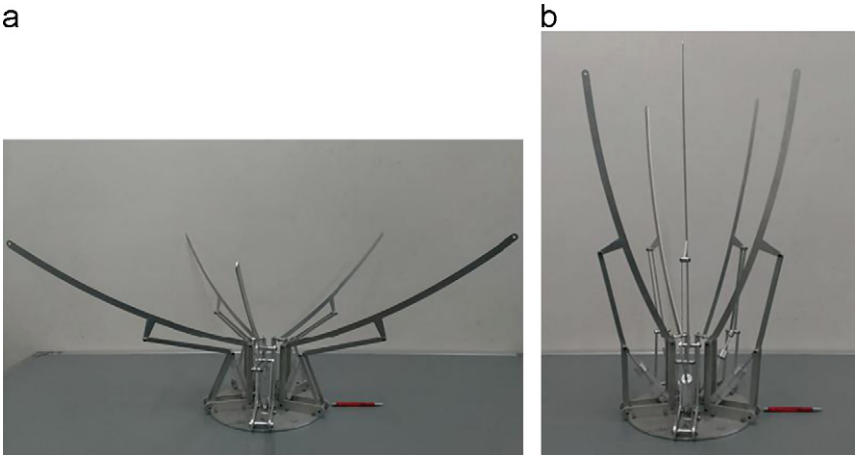

Fig. 12. A deployable mechanism of reflector compared with 13 cm red pen in (a) deployed state and (b) folded state. Thin-films, e.g. Kapton coated copper material, can be laid on surface of the five or more ribs. (For interpretation of the references to color in this figure legend, the reader is referred to the web version of this article.)

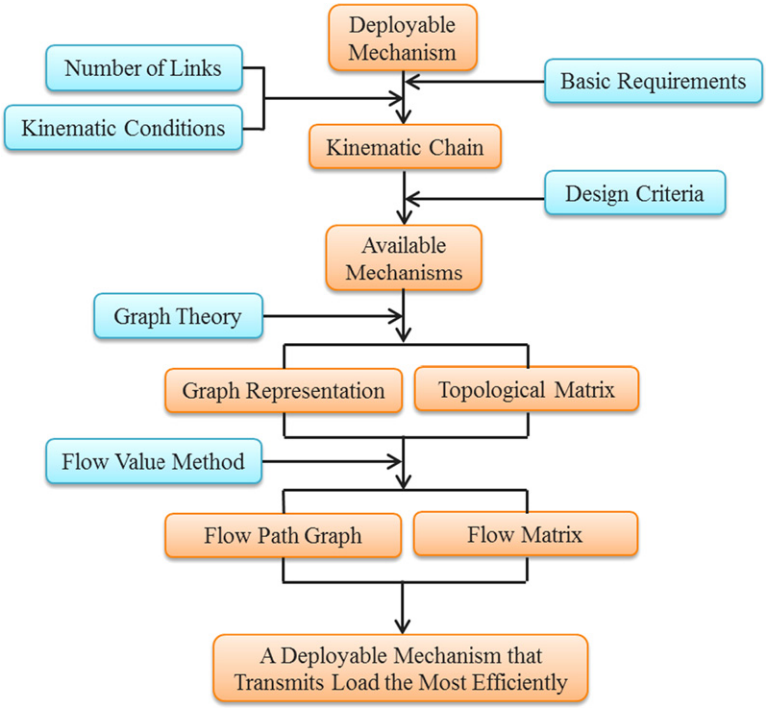

Fig. 13. Design process of deployable reflector.

reflector. This linkage corresponding to the mechanism in Fig. 6(c) is depicted in Fig. 11. As shown in Fig. 11, link 1 is the ground link and link 5 is the parabolic rib. Since link 3 is allowed to go in and out of link 2, the joint connecting these two links is treated as a translational joint. One end of link 3, link 4, and link 6 are combined into a multiple joint. The linkage complies with the aforementioned design requirements. Accordingly, as depicted in Fig. 12, five or more of linkages in a ring arrangement can constitute the deployable mechanism of a reflector. For aerospace antenna usages, on the surface of parabolic ribs, thin-films, e.g. Kapton® can in turn be pasted and copper material be coated [11,20]. This study has presented an effective methodology to design a deployable reflector. Fig. 13 summarizes the systematic design process.

References

[1] P. Gruber, S. Hauplik, B. Imhof, K. Ozdemir, R. Waclavicek, M.A. Perino, Deployable structures for a human lunar base, Acta Astronaut. 61 (2007) 484–495.

[2] R.E. McVey, S.F. Bassily, Apparatus and Method for Combined Redundant Deployment and Launch Locking of Deployable Satellite Appendages, U.S. Patent 5996940, 1999.

[3] I. Ohtomo, H. Kumazawa, T. Itanami, K. Ueno, A. Kondo, T. Yasaka, K. Nakajima, Y. Kawakami, M. Misawa, On-board multibeam deployable antennas using Ka, C, and S frequency bands, IEEE Trans. Aerosp. Electron. Syst. 28 (4) (1992) 990–1001.

[4] S.D. Guest, S. Pellegrino, A new concept for solid surface deployable antenna, Acta Astronaut. 38 (2) (1996) 103–113.

[5] R. Taylor, D. Turse, Large Aperture, Solid Surface Deployable Reflector, NASA NNX09AD57G, 2010.

[6] M.R. Johnson, The Galileo high gain antenna deployment anomaly, in: Proceedings of the 28th Aerospace Mechanisms Symposium, NASA Conference Publication CP-3260, 1994.

[7] S. Pellegrino, Deployable membrane reflectors, in: Proceedings of the 2nd World Engineering Congress, 2002 pp. 1–9.

[8] T. Takano, K. Miura, M. Natori, E. Hanayama, T. Inoue, T. Noguchi, N. Miyahara, H. Nakaguro, Deployable antenna with 10 m maximum diameter for space use, IEEE Trans. Antennas Propag. 52 (1) (2004) 2–11.

[9] J. Mitsugi, K. Ando, Y. Senbokuya, A. Meguro, Deployment analysis of large space antenna using flexible multibody dynamics simulation, Acta Astronaut. 47 (1) (2000) 19–26.

[10] Y. Sharay, U. Naftaly, TECSAR: design considerations and programme status, IEEE Proc. Radar, Sonar Navig. 153 (2) (2006) 117–121.

[11] C. Amend, M. Nurnberger, P. Oppenheimer, S. Koss, B. Purdy, A novel approach for a low-cost deployable antenna, in: Proceedings of the 40th Aerospace Mechanisms Symposium, 2010.

[12] P.G. Ingerson, W.C. Wong, The analysis of deployable umbrella parabolic reflectors, IEEE Trans. Antennas Propag. 20 (4) (1972) 409–414.

[13] J. Enders, S. Kas-Danouche, W. Liao, B. Rasmussen, T. Anh, K. Yokley, L. Robertson, R.C. Smith, Design of a membrane aperture deployable structure, in: Proceedings of the 44th AIAA/ASME/ASCE/AHS/ASC Structures, Structural Dynamics, and Materials Conference, 2003.

[14] A.V. Lopatin, E.V. Morozov, Modal analysis of the thin-walled composite spoke of an umbrella-type deployable space antenna, Compos. Struct. 88 (1) (2009) 46–55.

[15] T.S. Liu, C.C. Chou, Type synthesis of vehicle planner suspension mechanism using graph theory, J. Mech. Des. 115 (3) (1993) 652–657.

[16] H.S. Yan, Creative Design of Mechanical Devices, Springer, Singapore, 1998.

[17] C.H. Suh, C.W. Radcliffe, Kinematics and Mechanisms Design, John Wiley & Sons, New York, 1978.

[18] R.L. Norton, Design of Machinery: An Introduction to the Synthesis and Analysis of Mechanisms and Machines, McGraw Hill Higher Education, Boston, 2004.

[19] A.C. Rao, Selection of ground, input and output links in mechanisms: a quantitative approach, Trans. CSME 13 (1989) 23–29.

[20] DuPon™, Kapton® Polyimide Film, 〈http://www2.dupont.com/Kapton/en_US/〉.